REVIEW

Graphene family nanomaterials for application in cancer combination photothermal therapy

Duarte de Melo-Diogo, [iD] *†[a] Rita Lima-Sousa, [iD] †[a] Cátia G. Alves [iD] †[a] and Ilídio J. Correia [iD] *[a,b]

Combining hyperthermia with other therapies holds a great potential for improving cancer treatment. In this approach, the increase in the body temperature can exert a therapeutic effect on cells and/or enhance the effectiveness of anticancer agents. However, the conventional methodologies available to induce hyperthermia cannot confine a high temperature increase to the tumor-site while maintaining healthy tissues unexposed and ensuring minimal invasiveness. To overcome these limitations, combination photothermal therapy (PTT) mediated by graphene family nanomaterials (GFN) has been showing promising results. Such is owed to the ability of GFN to accumulate at the tumor site and convert near infrared light into heat, enabling a hyperthermia with a high spatial-temporal resolution. Furthermore, GFN can also incorporate different therapeutic agents on their structure for delivery purposes to cancer cells. In this way, the combination PTT mediated by GFN can result in an improved therapeutic effect. In this review, the combination of GFN mediated PTT with chemo-, photodynamic-, gene-, radio-, and immuno-therapies is examined. Furthermore, the main parameters that influence these types of combination approaches are also analyzed, with emphasis on the photothermal potential of GFN and on the vascular and cellular effects produced by the temperature increase mediated by GFN.

[a]CICS-UBI – Centro de Investigação em Ciências da Saúde, Universidade da Beira Interior, 6200-506 Covilhã, Portugal. E-mail: demelodiogo@fcsaude.ubi.pt, icorreia@ubi.pt

[b]CIEPQPF – Departamento de Engenharia Química, Universidade de Coimbra, Rua Sílvio Lima, 3030-790 Coimbra, Portugal

† These authors contributed equally to this article.

1. Introduction

Combining hyperthermia with radio- or chemo-therapies is a promising approach to improve cancer treatment.[1,2] In these therapeutic modalities, the increase in the body temperature (hyperthermia) can exert a therapeutic effect on cells and/or enhance the effectiveness of the other anticancer agents. In this way, the outcome of hyperthermia-based combination

Duarte de Melo-Diogo received his B.Sc. and M.Sc. degrees in Biomedical Sciences from Universidade da Beira Interior in 2012 and 2014, respectively. In 2018, Duarte de Melo-Diogo concluded his Ph.D. degree in Biochemistry from the same university. He is now a researcher at CICS-UBI research center. His research interests are focused on the biomedical application of graphene family nanomaterials and on the development of functional nanostructures for cancer therapy.

Duarte de Melo-Diogo

Rita Lima-Sousa received her B.Sc. in Biochemistry and M.Sc. in Biomedical Sciences from the Universidade da Beira Interior in 2016 and 2018, respectively. Currently, Rita Lima-Sousa is a Ph.D. student in Biochemistry at the same university. Her research interests are focused in the development and functionalization of graphene family nanomaterials for application in cancer photothermal therapy and biomedicine.

Rita Lima-Sousa

therapies is highly dependent on the maximum temperature achieved. However, the methodologies available to induce hyperthermia can limit its full therapeutic potential since these do not confine a high temperature increase to the tumor-site while maintaining healthy tissues unexposed and ensuring a minimal procedure invasiveness.[3,4]

To overcome these limitations, combination photothermal therapy (PTT) mediated by nanomaterials is a promising approach.[1,5–9] This type of therapy employs precisely engineered nanostructures that, due to their physicochemical properties, can achieve a high tumor accumulation.[10–13] Subsequently, the tumor zone is irradiated with laser light, and the nanomaterials' accumulated in this site interact with this radiation, producing an on-demand temperature increase.[12,14,15] The use of near infrared (750–1000 nm; NIR) light in these procedures is fundamental since it has minimal or insignificant interactions with biological components (e.g. water, collagen, melanin), thus ensuring a high penetration depth and minimal off-target heating.[5,12,16,17] Furthermore, these NIR-responsive nanomaterials may also accommodate other anticancer agents on their structure,[18–25] enabling the pursuit of synergistic therapeutic outcomes.

Among the different types of materials capable of being efficiently applied in combination PTT, graphene family nanomaterials (GFN) have been showing very promising results.[26–32] Such is owed to the GFN ability to absorb NIR light and convert it into heat, enabling a PTT with a high spatial-temporal resolution.[33–37] Furthermore, the aromatic lattice of GFN enables the direct loading of different agents (e.g. drugs, photosensitizers) on their structure for delivery purposes to cancer cells.[38–41] In this way, combining the photothermal and delivery capacities of GFN can result in an improved therapeutic effect.

In this review, the cancer combination PTT mediated by GFN is analyzed. Firstly, the synthesis and general properties of GFN are overviewed (section 2). Afterwards, the main parameters that influence the combination PTT mediated by GFN are reviewed (section 3), with emphasis on the photothermal potential of GFN (section 3.1), and on the vascular and cellular effects produced by the temperature increase mediated by GFN (section 3.2). Then, the combination of GFN mediated PTT with chemotherapy (section 4), photodynamic therapy (section 5), gene therapy (section 6), radiotherapy (section 7), and immunotherapy (section 8) is reviewed. Finally, an outlook about the state of the art and the future directions are presented in section 9. For the sake of simplicity, this review will not cover the application of GFN mediated PTT in conjugation with other photothermal agents (e.g. gold nanorods-GFN hybrids) nor with porous nanostructures with loading capacity (e.g. mesoporous silica-GFN hybrids).

2. GFN: synthesis and general properties

The members of the GFN are synthesized through different routes (extensively reviewed in ref. 42–44), originating materials with distinct properties that influence their application in cancer therapy.

Graphene oxide (GO) is commonly explored in photothermal applications and is also used as a precursor for the preparation of other GFN.[32] This nanomaterial is composed of a monolayer graphitic lattice incorporating several types of oxygen functional groups such as hydroxyl, carboxyl or epoxy (Fig. 1). The chemical oxidation of graphite and exfoliation of the attained material is the process usually employed to produce GO.[45,46] In this regard, the improved Hummers' method (uses H_2SO_4, H_3PO_4 and $KMnO_4$ for graphite oxidation) has been widely used to produce GO due to its high reaction yield.[46] The NIR absorption of GO allows its application in photothermal therapy (discussed in detail in section 3.1.). Furthermore, the aromatic lattice of this nanomaterial enables the direct loading of different therapeutic agents on its structure through hydrophobic–hydrophobic interactions and/or π–π stacking.[38,47–49]

GO can also be treated with reducing agents (e.g. hydrazine hydrate,[34,50] L-ascorbic acid,[51] glucose[52]) at 80–95 °C, yielding

Cátia G. Alves received her B.Sc. and M.Sc. degrees in Biomedical Sciences from Universidade da Beira Interior in 2016 and 2018, respectively. She is now a Ph.D. student in Biomedicine at the same university. Her research interests are focused on the application of NIR light responsive nanomaterials and small molecules in cancer theragnostic.

Cátia G. Alves

Ilídio J. Correia is an Associate Professor with habilitation in the Department of Health Sciences at Universidade da Beira Interior. He obtained his B.Sc. and Ph.D. degrees in Biochemistry from University of Lisbon in 1998 and New University of Lisbon in 2003, respectively. His research group is involved in the development of skin and bone substitutes, drug delivery systems, as well as in vitro 3D cell culture models aimed to reproduce solid tumors structural features.
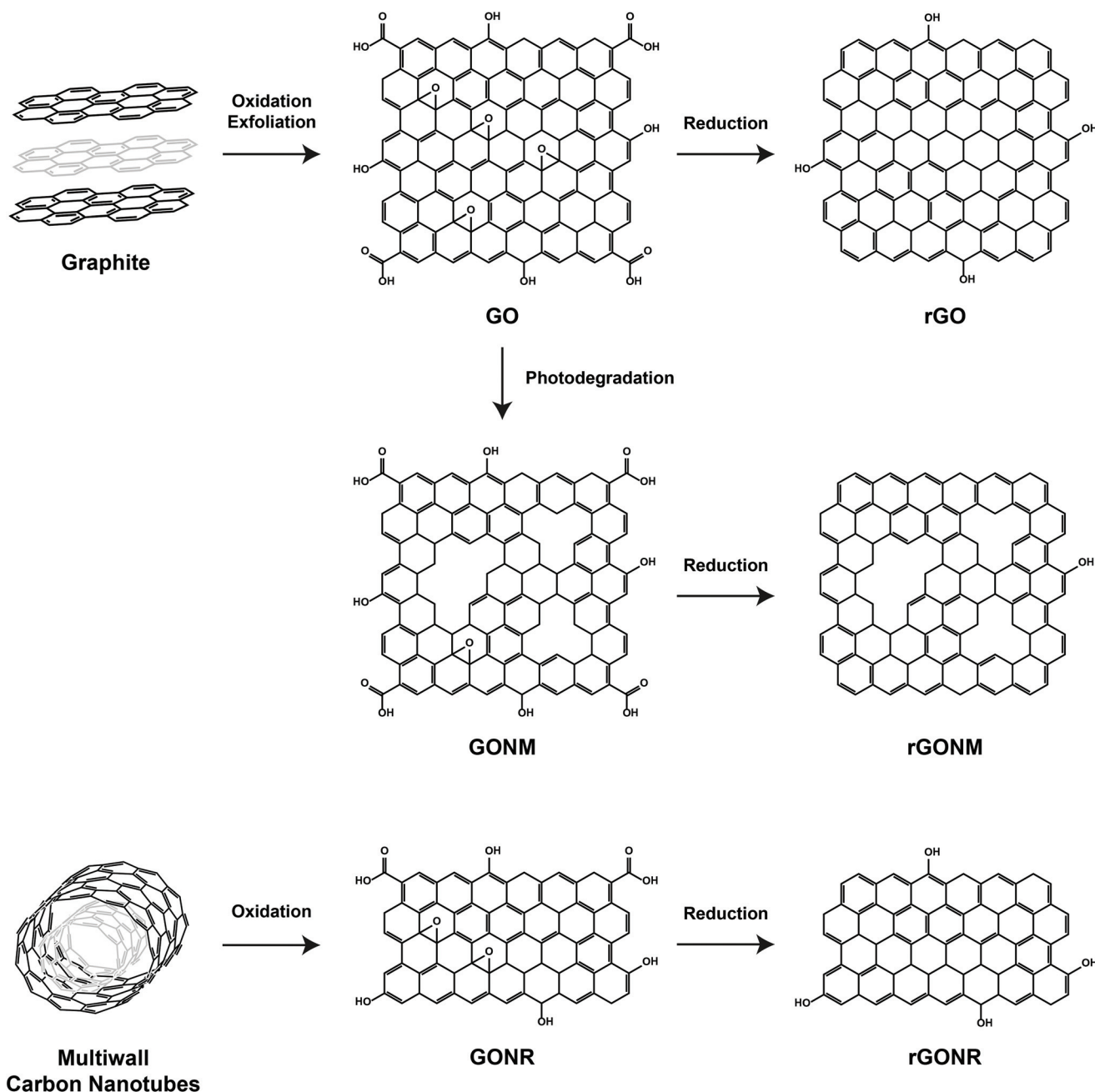
Ilídio J. Correia

Fig. 1 Synthesis routes of the members of the GFN.

reduced graphene oxide (rGO) (Fig. 1). This treatment intents to restore the graphitic aromatic lattice by removing the oxygen-functional groups, resulting in an improvement in the nanomaterials' NIR absorption.[32,34] When compared to GO, rGO also presents a higher drug loading capacity,[53,54] thereby being a promising agent for the delivery of therapeutics to cancer cells.

There are other GFN with a good photothermal potential but whose application in cancer therapy is not so widespread since their synthesis is more complex. This group includes graphene oxide nanoribbons (GONR), reduced graphene oxide

nanoribbons (rGONR) and reduced graphene oxide nanomesh (rGONM).

GONR are produced through the oxidation of multiwall carbon nanotubes (using $KMnO_4$ and H_2SO_4).[55,56] This process also leads to the unzipping of the nanotubes (Fig. 1).[55,56] The chemical treatment of GONR with reducing agents (e.g. hydrazine hydrate) generates rGONR, which also display an enhanced NIR absorption.[55]

rGONM is produced through the photodegradation of GO (using TiO_2 nanoparticles immobilized on a SiO_2-film and radiation from a mercury lamp) and subsequent reduction

(using hydrazine hydrate) of the attained material (Fig. 1).[57] The use of rGONM for cancer PTT is also appealing due to its improved NIR absorption.[57]

Nevertheless, the as-synthesized GFN present critical limitations that hinder their direct application in cancer therapy. Even though GO based materials have some water solubility (due to their oxygen-functional groups), these materials precipitate in saline solutions and biological fluids.[32,34] Several reports have shown that as-synthesized GO based materials can present a cytocompatible profile *in vitro* (which is dependent on multiple factors, such as materials' physicochemical properties, impurities, presence of serum).[32] However, the *in vivo* intravenous administration of GO leads to its accumulation and retention in the lungs, inducing severe effects on this organ.[58] The rGO derivatives display limited water solubility and also precipitate in biological-relevant media.[32,34] Furthermore, rGO derivatives are highly cytotoxic, a fact that can be attributed to their insolubility and contamination with traces of hydrazine hydrate (a highly toxic reducing agent used in the majority of the protocols followed to produce rGO derivatives).[32,52]

The limitations of as-synthesized GFN can be surpassed by functionalizing them with materials (*e.g.* hydrophilic polymers) capable of enhancing nanostructures' colloidal stability and biocompatibility (extensively reviewed by our group in ref. 32). In this way, the functionalization of GFN enables their application in cancer therapy.[32] For this purpose, the carboxyl groups of GO based materials can be covalently bond to primary amine-terminated polymers using the carbodiimide chemistry.[32,34,59] In this regard, Yang *et al.* demonstrated that GO derivatives functionalized with amine-terminated branched poly(ethylene glycol) (PEG) did not induce any toxicity to mice when administered by intravenous, intraperitoneal and oral routes, thus displaying an excellent biocompatibility *in vivo*.[59,60] Similar findings were also observed for GO functionalized with amine-terminated Dextran.[61] On the other hand, the aromatic lattice of the rGO based materials can be functionalized with amphiphilic polymers through hydrophobic-hydrophobic interactions and/or π–π stacking.[32,34,51,55,57] In this regard, rGO functionalized with PEGylated poly(maleic anhydride-*alt*-1-octadecene) and bovine serum albumin also displayed a biocompatibility profile suitable for *in vivo* applications.[60,62,63]

3. GFN mediated combination PTT

The application of GFN in cancer combination PTT generally starts with the administration of these nanomaterials through intravenous injection.[62,64–66] After entering into the blood circulation, GFN can accumulate in the tumor zone by taking advantage from the tumor's leaky vasculature (enhanced permeability and retention (EPR) effect) and from the dynamic vents that spontaneously occur in the tumor associated vessels.[32,67,68] Subsequently, the tumor zone is exposed to NIR light and the GFN convert the absorbed radiation into

heat.[32,34] In this way, GFN can confine the hyperthermia to this site and elicit minimal off-target heating.[12,32] The attained temperature increase in the tumor zone can *per se* induce damage on cancer cells and/or sensitize them to the action of other agents, leading to an improved therapeutic outcome.

In this way, the combination PTT mediated by GFN depends strongly on three factors: (i) the ability of GFN to reach the tumor zone, (ii) the intrinsic photothermal capacity of each member of the GFN and (iii) the temperature variation achieved, upon laser irradiation, at the tumor site.

The ability of GFN to effectively reach the tumor zone is dependent on the nanostructures' physicochemical properties, namely on their size, charge, corona composition and decoration with targeting ligands.[32] These properties and considerations regarding GFN biodistribution were recently analyzed by our group and by other research teams (reviewed in detail in ref. 32 and 69–71). In turn, the photothermal capacity of GFN is influenced by the NIR absorption of each derivative (reviewed in section 3.1), while the therapeutic outcome of the combination PTT is affected by the local temperature variation achieved upon irradiation (reviewed in section 3.2).

3.1. Photothermal capacity of GFN

The members of GFN have different capabilities to absorb the NIR radiation, ultimately impacting their photothermal capacity and hence their potential for combination PTT.

Due to its NIR absorption, GO can produce a temperature increase upon interaction with NIR light. The attained temperature variation is dependent on the concentration of GO and on the laser related parameters (*e.g.* intensity, duration).[23,72]

The reduction of GO restores the nanostructures' aromatic lattice, thus improving their NIR absorption and photothermal potential.[32,34] In this regard, Yang *et al.* demonstrated that rGO based materials can display a 3–4 fold higher NIR absorption than GO derivatives.[34] Consequently, the GO derivatives could produce a temperature increase to about 44 °C under NIR laser irradiation, while the rGO based materials induced a photoinduced heat to ≈58 °C (808 nm, 1 W cm^{-2}, 5 min).[34] However, the manipulation of rGO based materials is not straightforward. The rGO derivatives can aggregate irreversibly during the reduction phase, thus requiring additional processing steps.[34,50] Furthermore, the use of rGO demands additional purification routines to ensure the removal of the reducing agents, some of which are cytotoxic.[34,73] Due to these reasons, GO derivatives are still widely explored in cancer PTT.

The other GFN can display an enhanced photothermal capacity. GONR present a NIR absorption similar to that of GO based materials.[55] In contrast, rGONR based materials can display a ≈2.4-fold higher absorption at 808 nm than rGO derivatives.[55] Such phenomenon was attributed to the higher abundance of low-energy vibrational modes in rGONR arising from their intrinsic shape.[55] Due to their higher NIR absorption, the rGONR based materials could produce a temperature increase up to ≈61 °C under NIR laser irradiation, while the rGO derivatives only raised the temperature to ≈46 °C (808 nm, 7.5 W cm^{-2}, 10 min).[55]

Akhavan *et al.* demonstrated that rGONM displays a 4.2-fold higher NIR absorption than rGO based materials.[57] A greater restoration of rGONM aromatic lattice and/or a higher abundance of low-energy vibrational modes in this nanomaterial can explain its enhanced NIR absorption.[55,57] Due to this fact, rGONM can produce a photoinduced heat to ≈57 °C (808 nm, 0.1 W cm^{-2}, 8 min).[57] Under the same conditions, the rGO based materials only produced a temperature increase to about 42 °C.[57]

3.2. Effect of the temperature increase mediated by GFN

The local temperature increase mediated by GFN upon NIR laser irradiation will dictate the therapeutic outcome of the combination PTT. Depending on the temperature achieved, the photoinduced heat mediated by GFN can induce irreversible or reversible damage on cells. In this context, achieving a photoinduced heat to about 50 °C can *per se* induce irreversible damage on cells, causing protein denaturation, collapse of cells' membrane, and dysfunctions on the activity of enzymes and mitochondria.[74] These events ultimately lead to cells' death by coagulative necrosis.[74]

On the other hand, a local temperature increase to about 41–45 °C can *per se* induce sub-lethal and reversible damage on cells by compromising cells' metabolism and DNA repair mechanisms.[74,75] Furthermore, this temperature range can also sensitize cells to the action of other therapeutics or enhance therapeutics' efficacy, leading to an improved outcome.[75]

Mild hyperthermia can increase the blood flow into the tumor tissue, improving tissues' oxygenation.[75,76] Moreover, this increased blood flow can also augment the amount of GFN that reach the tumor zone (hyperthermia enhanced EPR
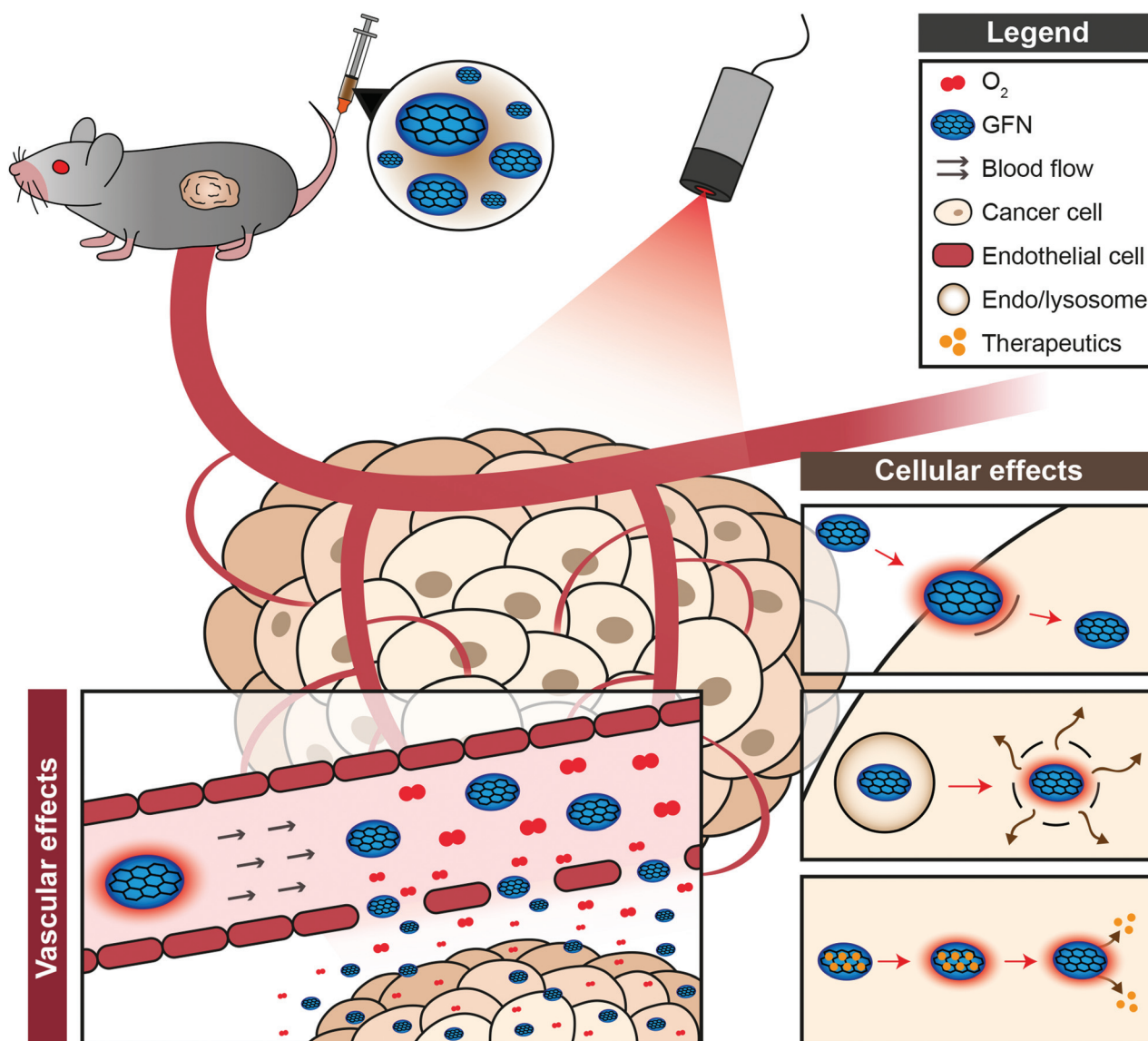

Fig. 2 Illustration of the vascular and cellular effects of GFN mediated photoinduced heat.

Table 1 Combination PTT mediated by GFN: *in vivo* results

GFN	Modality	Tumor model	Administration route	Dose	Laser parameters	Tumor temperature[o]	Outcome of combination therapy	Outcome of stand-alone therapies	Ref.
DOX loaded lactoferrin/rGO based nanocapsules	Chemo-PTT	RG2 tumor bearing mice	i.v.[a]	DOX loaded lactoferrin/rGO based nanocapsules: 25 mg kg⁻¹; DOX: 1.28 mg kg⁻¹	808 nm, 2 W cm⁻², 5 min	55 °C (808 nm, 2 W cm⁻², 3 min)	Tumor eradication	Lactoferrin/rGO based nanocapsules + NIR: tumor growth reduction. Free DOX: tumor growth reduction	83
EPI[b] loaded Cetuximab-PEG-GO	Chemo-PTT	U87 tumor bearing mice	i.v.	EPI loaded Cetuximab-PEG-GO: 6 mg kg⁻¹; EPI: 3 mg kg⁻¹; Cetuximab: 0.2 mg kg⁻¹	808 nm, 2 W cm⁻², 2 min	88 °C	Tumor eradication	EPI loaded Cetuximab-PEG-GO: tumor growth reduction. EPI loaded PEG-GO: tumor growth reduction. Free EPI: tumor growth reduction	64
Platinum-PEG-GO complex	Chemo-PTT	4T1 tumor bearing mice	i.v.	Platinum: 10 mg kg⁻¹ (twice)	785 nm, 1.5 W cm⁻², 3 min (twice)	N.A.	Tumor eradication	PEG-GO + NIR: tumor growth inhibition. Platinum-PEG-GO complex: tumor growth reduction. Cisplatin: tumor growth reduction	77
RV[c] loaded mPEG[d]/rGO	Chemo-PTT	4T1 tumor bearing mice	i.t.[e]	GO: 10 mg kg⁻¹; RV: 18 mg kg⁻¹	808 nm, 0.6 W cm⁻², 5 min	70 °C	Tumor eradication	mPEG/rGO + NIR: tumor growth reduction. Free RV: tumor growth reduction	54
DOX loaded mPEG-GO	Chemo-PTT	EMT6 tumor bearing mice	i.v.	DOX: 10 mg kg⁻¹	808 nm, 2 W cm⁻², 5 min	50 °C (i.t.)	Tumor eradication (in 4 out of 5 mice)	mPEG-GO + NIR: tumor growth reduction. Free DOX: tumor growth reduction	95
MIT[f] loaded HA[g]-GO	Chemo-PTT	MCF-7 tumor bearing mice	i.v.	MIT: 4 mg kg⁻¹ (every 2 days for 7 days)	808 nm, 2 W cm⁻², 1 min (every 2 days for 7 days)	N.A.	Tumor regression	HA-GO + NIR: tumor growth reduction. Free MIT + NIR: tumor growth inhibition	65
DSPE-PEG[h]-NGR[i]/DOX-GO@Ag nanocomposite	Chemo-PTT	S180 tumor bearing mice	i.v.	DSPE-PEG-NGR/GO@Ag: 6.1 mg kg⁻¹; DOX: 5 mg kg⁻¹ (every 2 days)	808 nm, 2 W cm⁻², 3 min (every 2 days)	N.A.	Tumor regression	DSPE-PEG-NGR/GO@Ag + NIR: tumor growth reduction. DSPE-PEG-NGR/DOX-GO@Ag; tumor growth reduction. Free DOX: tumor growth reduction	85
RV loaded PEGDE[j]/GO	Chemo-PTT	4T1 tumor bearing mice	i.t.	GO: 10 mg kg⁻¹; RV: 18 mg kg⁻¹	808 nm, 0.6 W cm⁻², 5 min	47 °C	Tumor growth reduction	PEGDE/GO + NIR: tumor growth reduction. Free RV: tumor growth reduction	54

Table 1 (Contd.)

GFN	Modality	Tumor model	Administration route	Dose	Laser parameters	Tumor temperature[o]	Outcome of combination therapy	Outcome of stand-alone therapies	Ref.
DOX loaded HA-SS-GO	Chemo-PTT	MDA-MB-231 tumor bearing mice	i.v.	DOX: 2 mg kg⁻¹ (every 3 days for 18 days)	808 nm, 5 W cm⁻², 10 min (every 3 days for 18 days)	N.A.	Tumor growth reduction	HA-SS-GO + NIR: tumor growth reduction; DOX loaded HA-SS-GO: tumor growth reduction; Free DOX: tumor growth reduction	84
Methylene blue loaded Pluronic F127/GO	Photodynamic-PTT	4T1-Luc tumor bearing mice	i.t.	Pluronic F127/GO: 10 mg kg⁻¹; Methylene blue: 2.5 mg kg⁻¹ (3 times)	660 nm, 90.8 J cm⁻², 10 min; 808 nm, 8.3 kJ cm⁻², 15 min (3 times)	70 °C (808 nm, 8.3 kJ cm⁻², 3 min)	Tumor eradication	Methylene blue loaded Pluronic F127/GO + NIR: tumor growth reduction; Methylene blue loaded Pluronic F127/GO + 660 nm: tumor growth reduction	89
IR808-bPEI[k]-PEG-GO	Photodynamic-PTT	A549 tumor bearing mice	i.v.	IR808-bPEI-PEG-GO: 10 mg kg⁻¹; bPEI-PEG-GO: 8 mg kg⁻¹; IR808: 2 mg kg⁻¹	808 nm, 1 W cm⁻², 5 min	59 °C	Tumor eradication	bPEI-PEG-GO + NIR: tumor growth reduction; Free IR808 + NIR: tumor growth reduction	66
Methylene blue loaded Pluronic F127/GO	Photodynamic-PTT	HeLa tumor bearing mice	i.v.	Pluronic F127/GO: 10 mg kg⁻¹; Methylene blue: 2 mg kg⁻¹	650 nm, ≈150 mW cm⁻², 10 min; 808 nm, 2 W cm⁻², 3 min	50 °C	Tumor eradication	Methylene blue loaded Pluronic F127/GO + NIR: tumor growth reduction; Methylene blue loaded Pluronic F127/GO + 650 nm: tumor growth reduction	87
PEG-Ru(II) complex loaded rGO	Photodynamic-PTT	A549 tumor bearing mice	i.t.	PEG-Ru(II) complex loaded rGO: 5 µg g⁻¹	808 nm, 0.5 W cm⁻², 5 min; 450 nm, 20 mW cm⁻², 2 min	59 °C	Tumor regression	PEG-Ru(II) complex loaded rGO + NIR: tumor growth reduction; PEG-Ru(II) complex loaded rGO + 450 nm: tumor growth reduction	88
HDAC1 and K-Ras siRNA complexed PAH/folic acid-PEG-GO	Gene-PTT	MIA PaCa-2 tumor bearing mice	i.p.[l]	PAH/folic acid-PEG-GO: 4 mg kg⁻¹; HDAC1 siRNA: 16 µg K-Ras siRNA: 16 µg (once every 4 days)	808 nm, 1 W cm⁻², 1 min (once every 4 days)	N.A.	Tumor growth reduction	PAH/folic acid-PEG-GO + NIR: tumor growth reduction; HDAC1 and K-Ras siRNA complexed PAH/folic acid-PEG-GO: tumor growth reduction	90
¹³¹I labeled C₁₈PMH[m]-PEG/rGO	Radio-PTT	4T1 tumor bearing mice	i.v.	¹³¹I labeled C₁₈PMH-PEG/rGO: 10 mg kg⁻¹; ¹³¹I: 200 µCi	808 nm, 0.2 W cm⁻², 20 min	45–46 °C	Tumor eradication (in 4 out of 5 mice)	¹³¹I labeled C₁₈PMH-PEG/rGO: tumor growth reduction; ¹³¹I: tumor growth reduction	62

Table 1 (Contd.)

GFN	Modality	Tumor model	Administration route	Dose	Laser parameters	Tumor temperature[o]	Outcome of combination therapy	Outcome of stand-alone therapies	Ref.
PVP[n]/BiP$_5$W$_{30}$-rGO	Radio-PTT	HeLa tumor bearing mice	i.t.	PVP/BiP$_5$W$_{30}$-rGO: 40 µg X-ray: 6 Gy	808 nm, 0.35 W cm^{-2}, 10 min	45 °C	Tumor eradication (in 1 out of 4 mice)	PVP/BiP$_5$W$_{30}$-rGO + NIR: tumor growth reduction PVP/BiP$_5$W$_{30}$-rGO + X-ray: tumor growth reduction X-ray: tumor growth reduction	76
CpG ODNs complexed PEI-PEG-GO	Immuno-PTT	CT26 tumor bearing mice	i.t.	PEI-PEG-GO: 2 mg kg^{-1} CpG ODNs: 180 µg kg^{-1}	808 nm, 2 W cm^{-2}, 5 min	50 °C	Tumor regression	PEI-PEG-GO + NIR: tumor growth reduction CpG ODNs complexed PEI-PEG-GO: tumor growth reduction CpG ODNs: tumor growth reduction	79

[a] Intravenous (i.v.), [b] Epirubicin (EPI), [c] Resveratrol (RV), [d] MethoxyPEG (mPEG), [e] Intratumoral (i.t.), [f] Mitoxantrone (MIT), [g] Hyaluronic acid (HA), [h] 1,2-Distearoyl-sn-glycero-3-phosphoethanolamine-N-PEG (DSPE-PEG), [i] Asn-Gly-Arg peptide (NGR), [j] PEG dimethyl ether (PEGDE), [k] Branched PEI (bPEI), [l] Intraperitoneal (i.p.), [m] Poly(maleic anhydride-alt-1-octadecene) (C$_{18}$PMH), [n] Poly(vinyl pyrrolidone) (PVP). [o] The value of the tumor's temperature is approximate. Not available (N.A.).

effect).[77] As a result of the mild hyperthermia, cells' membrane permeability is also affected.[75,78] In this way, the temperature increase produced by GFN upon NIR laser irradiation can improve nanomaterials' cellular uptake.[40,72,79] The photoinduced heat generated by GFN can also disrupt the endosomes/lysosomes, prompting the delivery of the loaded agents to the cytoplasm.[53,80] Additionally, the interaction of the GFN with NIR light can trigger the intracellular release of the loaded therapeutics.[54] By taking advantage from these mechanisms (illustrated in Fig. 2) and from the effects of the hyperthermia *per se*, GFN mediated PTT can improve the therapeutic outcome of different types of therapies (reviewed in the following sections).

4. PTT mediated by GFN in combination with chemotherapy

The aromatic lattice of GFN allows the direct loading of chemotherapeutics on their structure through hydrophobic–hydrophobic interactions and/or π–π stacking.[81,82] In this way, GFN can be explored to control the delivery of drugs to cancer cells. Chen *et al.* demonstrated that the NIR light can trigger the release of resveratrol from rGO based materials inside cancer cells.[54] By exposing cells to NIR light for 10 min, the intracellular release of this drug increased from about 3% to ≈30%.[54] Such behavior can be attributed to the detachment of the drugs from GFN due to the local temperature increase achieved upon NIR laser irradiation.[54,83] Additionally, the photoinduced heat generated by both GO and rGO based materials can also disrupt the endo/lysosomes,[53,84] further contributing to the release of the loaded drugs in the cytoplasm.

By taking advantage from these two phenomena and from the cellular effects of the hyperthermia *per se*, GFN mediated chemo-PTT can lead to improved therapeutic outcomes (Tables 1 and 2). For instance, Thapa and co-workers verified that the chemo-PTT mediated by folic acid-functionalized rGO co-loaded with irinotecan and docetaxel could reduce MCF-7 cells' viability to about 24%.[81] In stark contrast, the sole application of the dual drug loaded rGO based material (chemotherapeutic effect) or the conjugation of the rGO based material with NIR light (photothermal effect) only decreased cells' viability to about 64 and 84%, respectively.[81] In another work, Feng *et al.* verified that the delivery of doxorubicin (DOX) through PEGylated pH-responsive GO to DOX-resistant MCF-7 cells could reduce their viability to about 55% (Fig. 3).[82] In turn, the chemo-photothermal effect mediated by the DOX loaded GFN reduced cells' viability to about 21%,[82] proving to be a promising agent for the elimination of drug-resistant cancer cells.

The hyperthermia induced by GFN can also enhance nanostructures' ability to deliver drugs to the tumor tissue. In this regard, Li *et al.* verified that the delivery of a platinum complex by PEGylated GO would result in a platinum tumor accumulation of 9.6 µg g^{-1} (Fig. 4).[77] In contrast, mice treated with the platinum-PEG-GO complex plus NIR light presented a platinum

Table 2 Combination PTT mediated by GFN: *in vitro* results

GFN	Modality	Cell line	Dose	Laser parameters	Cell viability after combination therapy[o]	Cell viability after stand-alone therapies[o]	Ref.
DOX loaded DSPE-PEG-NH$_2$/GONR	Chemo-PTT	U87 cells	DOX: ≈16.6 µg mL^{-1}	808 nm, 2 W cm^{-2}, 2 min	2%	DOX loaded DSPE-PEG-NH$_2$/GONR: 36%, Free DOX: 59%	96
EPI loaded Cetuximab-PEG-GO	Chemo-PTT	U87 cells	EPI: ≈14 µg mL^{-1}	808 nm, 2 W cm^{-2}, 2 min	2%	EPI loaded Cetuximab-PEG-GO: 14%, Free EPI: 55%	64
Platinum-PEG-GO complex	Chemo-PTT	4T1 cells	PEG-GO: 890 µg mL^{-1} Pt: 100 µM	785 nm, 1.5 W cm^{-2}, 3 min	2%	PEG-GO + NIR: 8%, Platinum-PEG-GO complex: 13%, Free Pt(II): 24%	77
MIT loaded HA-GO	Chemo-PTT	MCF-7 cells	MIT: 51.2 µg mL^{-1}	808 nm, 2 W cm^{-2}, 3 min	3%	HA-GO + NIR: 40%, MIT loaded HA-GO: 14%, Free MIT: 23%	65
DSPE-PEG-NGR/DOX-GO@Ag nanocomposite	Chemo-PTT	MCF-7 cells	DOX: 4 µg mL^{-1}	808 nm, 2 W cm^{-2}, 3 min	6%	DSPE-PEG-NGR/DOX-GO@Ag nanocomposite: 36%, Free DOX: 37%	85
DOX loaded lactoferrin/rGO based nanocapsules	Chemo-PTT	RG2 cells	DOX: 0.25 µg mL^{-1}	808 nm, 2 W cm^{-2}, 5 min	6%	Lactoferrin/rGO based nanocapsules + NIR: 84%, DOX loaded lactoferrin/rGO based nanocapsules: 87%, Free DOX: 51%	83
TPGS^a/rGO	Chemo-PTT	MCF-7 cells	rGO: 10 µg mL^{-1}	808 nm, 1.7 W cm^{-2}, 5 min	6%	TPGS/rGO: 37%	23
Sorafenib loaded PVP/FA^b-GO	Chemo-PTT	KB cells	Sorafenib: 100 µM	NIR, 3 W cm^{-2}, 5 min	7%	PVP/FA-GO + NIR: 82%, Sorafenib loaded PVP/FA-GO: 16%, Free Sorafenib: 26%	97
TPGS/GO	Chemo-PTT	MCF-7 cells	GO: 10 µg mL^{-1}	808 nm, 1.7 W cm^{-2}, 5 min	8%	TPGS/GO: 75%	23
DOX loaded PVP/FA-GO	Chemo-PTT	HeLa cells	DOX: 20 µg mL^{-1}	808 nm, 2 W cm^{-2}, 5 min	10%	DOX loaded PVP/FA-GO: 29%, Free DOX: 30%	98
DOX loaded mPEG-GO	Chemo-PTT	EMT6 cells	DOX: 30 µg mL^{-1}	808 nm, 2 W cm^{-2}, 3 min	10%	mPEG-GO + NIR: 17%, Free DOX: 21%	95
DOX loaded DA-PAH^c-PEG-GO	Chemo-PTT	MCF-7/ADR cells	GO: ≈40 µg mL^{-1} DOX: 20 µg mL^{-1}	808 nm, 0.5 W cm^{-2}, 5 min	21%	DA-PAH-PEG-GO + NIR: 74%, DOX loaded DA-PAH-PEG-GO: 55%, Free DOX: 88%	82
DOX loaded PEG-bPEI-rGO	Chemo-PTT	HeLa cells	DOX: 50 µg mL^{-1}	808 nm, 6 W cm^{-2}, 30 min	22%	DOX loaded PEG-bPEI-rGO: 56%, Free DOX: 9%	53
DOX loaded HA-SS-GO	Chemo-PTT	MDA-MB-231	DOX: 5 µg mL^{-1}	808 nm, 5 W cm^{-2}, 5 min	22%	HA-SS-GO + NIR: 73%, DOX loaded HA-SS-GO: 33%	84
IRI^d and DOC^e loaded FA-P407^f/rGO	Chemo-PTT	MCF-7 cells	IRI + DOC: 100 µM	NIR, 3 W cm^{-2}, 5 min	24%	FA-P407/rGO + NIR: 84%, IRI and DOC loaded FA-P407/rGO: 64%, Free IRI + DOC: 74%	81
DOX and IRI loaded P188^g/GO	Chemo-PTT	SCC-7 cells	GO: ≈6 µg mL^{-1} DOX + IRI: 1 µg mL^{-1}	808 nm, 3 W cm^{-2}, 5 min	35%	P188/GO + NIR: 67%, DOX and IRI loaded P188/GO: 66%, Free DOX + IRI: 64%	99
DOX and TOS^h loaded C$_{18}$PMH-POx^j/GO	Chemo-PTT	MCF-7 cells	GO: 34.7 µg mL^{-1} DOX + TOS: 20.5 µM	808 nm, 1.7 W cm^{-2}, 5 min	39%	DOX and TOS loaded C$_{18}$PMH-POx/GO: 61% Free DOX + TOS: 74%	49
RV loaded mPEG/rGO	Chemo-PTT	4T1 cells	GO: 22 µg mL^{-1} RV: 40 µg mL^{-1}	808 nm, 0.6 W cm^{-2}, 3 min	55%	mPEG/rGO + NIR: 99%, RV loaded mPEG/rGO: 65%	54

Table 2 (Contd.)

GFN	Modality	Cell line	Dose	Laser parameters	Cell viability after combination therapy[o]	Cell viability after stand-alone therapies[o]	Ref.
RV loaded PEGDE/GO	Chemo-PTT	4T1 cells	RV: 50 μg mL⁻¹	808 nm, 0.6 W cm⁻², 3 min	71%	RV loaded PEGDE/GO: 80%	54
IR808-bPEI-PEG-GO	Photodynamic-PTT	Lewis cells	IR808: 10 μM	808 nm, 2 W cm⁻², 5 min	0%	bPEI-PEG-GO + NIR: 75%; Free IR808 + NIR: 38%	66
Ce6 loaded PEG-GO	Photodynamic-PTT	KB cells	Ce6: 2.5 μM	808 nm, 0.3 W cm⁻², 20 min; 660 nm, 0.05 W cm⁻², 5 min	2%	Ce6 loaded PEG-GO + NIR: 83%; Ce6 loaded PEG-GO + 660 nm: 25%; Free Ce6 + 660 nm: 100%	40
Methylene blue loaded Pluronic F127/GO	Photodynamic-PTT	4T1 cells	Pluronic F127/GO: 12.5 μg mL⁻¹; Methylene blue: 2.5 μg mL⁻¹	660 nm, 34 J cm⁻², 3 min; 808 nm, 1.65 kJ cm⁻², 3 min	5%	Methylene blue loaded Pluronic F127/GO + 660 nm: 4%; Pluronic F127/GO + NIR: 66%; Free MB + 660 nm: 4%	89
PEG-Ru(II) complex loaded rGO	Photodynamic-PTT	A549 cells	PEG-Ru(II) complex: 6.25 μM	808 nm, 0.5 W cm⁻², 5 min; 450 nm, 20 mW cm⁻², 2 min	8%	PEG-Ru(II) complex loaded rGO + NIR: 18%; PEG-Ru(II) complex loaded rGO + 450 nm: 52%	88
ZnPc[j] loaded UCNPs[k]-PEG-GO	Photodynamic-PTT	HeLa cells	ZnPc loaded UCNPs-PEG-GO: 80 μg mL⁻¹	808 nm, 2 W cm⁻², 10 min; 630 nm, 50 mW cm⁻², 10 min	16%	ZnPc loaded UCNPs-PEG-GO + NIR: 74%; ZnPc loaded UCNPs-PEG-GO + 630 nm: 50%	86
Methylene blue loaded Pluronic F127/GO	Photodynamic-PTT	HeLa cells	Pluronic F127/GO: 10 μg mL⁻¹; Methylene blue: 2 μg mL⁻¹	655 nm, ≈150 mW cm⁻², 3 min; 808 nm, 2 W cm⁻², 3 min	23%	Pluronic F127/GO + NIR: 41%; Methylene blue loaded Pluronic F127/GO + 655 nm: 49%; Free Methylene blue + 655 nm: 57%	87
C₆₀[l]-mPEG-GO	Photodynamic-PTT	HeLa cells	GO: 40 μg mL⁻¹; C₆₁(COONa)₂: 10.4 μg mL⁻¹	808 nm, 4 W cm⁻², 7 min	59%	mPEG-GO + NIR: 78%; Free C₆₁(COONa)₂ + NIR: 81%	100
¹³¹I labeled C₁₈PMH-PEG/rGO	Radio-PTT	4T1 cells	C₁₈PMH-PEG/rGO: 100 μg mL⁻¹; ¹³¹I: 100 μCi mL⁻¹	808 nm, 0.5 W cm⁻², 10 min	6%	C₁₈PMH-PEG/rGO + NIR: 87%; ¹³¹I labeled C₁₈PMH-PEG/rGO: 50%; Free ¹³¹I: 89%	62
IUdR loaded PLGA[m]/GO	Radio-PTT	U87MG cells	IUdR loaded PLGA/GO: 80 μg mL⁻¹; IUdR: 0.35 μg mL⁻¹; X-ray: 2 Gy	808 nm, 2 W cm⁻², 3 min;	29%[n]	PLGA/GO + NIR: 63%[n]; IUdR loaded PLGA/GO + X-ray: 38%[n]; Free IUdR + X-ray: 55%[n]	93

[a] α-Tocopherol polyethylene glycol 1000 succinate (TPGS). [b] Folic acid (FA). [c] 2,3-Dimethylmaleic anhydride modified PAH (DA-PAH). [d] Irinotecan (IRI). [e] Docetaxel (DOC). [f] Poloxamer 407 (P407). [g] Poloxamer 407 (P188). [h] D-α-Tocopherol succinate (TOS). [i] Poly(2-ethyl-2-oxazoline) (POx). [j] Zinc phthalocyanine (ZnPc). [k] Upconversion nanoparticles (UCNP). [l] Fullerene (C₆₀). [m] Poly (lactide-co-glycolide) (PLGA). [n] Plating efficiency. [o] The values of the cells' viability are approximated.
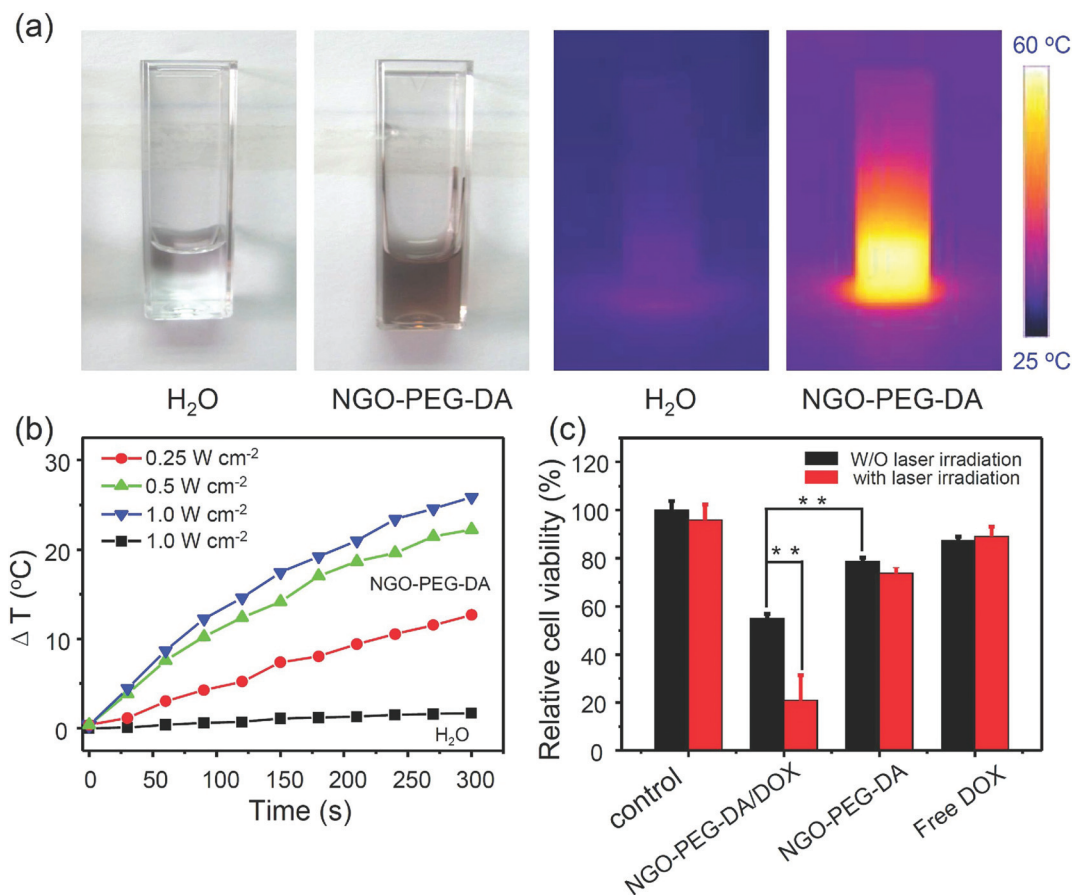
Fig. 3 Properties of DOX loaded PEG functionalized pH-responsive GO. (a) Optical and infrared thermal images of water and PEG functionalized pH-responsive GO upon exposure to NIR light (808 nm, 1 W cm^{-2}, 5 min). (b) Temperature variation curves of PEG functionalized pH-responsive GO upon NIR laser irradiation. (c) Chemo-PTT effect mediated by DOX loaded PEG functionalized pH-responsive GO towards DOX-resistant MCF-7 cells (808 nm, 0.5 W cm^{-2}, 5 min; with laser irradiation). DOX loaded PEG functionalized pH-responsive GO (NGO-PEG-DA/DOX), PEG functionalized pH-responsive GO (NGO-PEG-DA). Copyright © 2014 by John Wiley & Sons, Inc. Reprinted from ref. 82 by permission of John Wiley & Sons, Inc.

tumor uptake of 13.3 µg g^{-1}.[77] As a result, the chemo-PTT mediated by platinum-PEG-GO complex induced tumors' eradication while the sole application of chemotherapy (platinum or platinum-PEG-GO complex) or PTT (PEG-GO + NIR) only led to a reduction or inhibition of the tumors' growth, respectively.[77] A similar observation was reported by Shi *et al.*, which verified that the DOX released in the tumor tissue of mice treated with a DOX-GO based conjugate could be increased by about 1.65 times upon NIR laser irradiation.[85]

5. PTT mediated by GFN in combination with photodynamic therapy

GFN aromatic structure can incorporate photosensitizers for application in combination photodynamic-PTT. For this purpose, chlorin e6 (Ce6) and phthalocyanine derivatives have been adsorbed on GFN surface by taking advantage from hydro-

phobic–hydrophobic interactions and/or π–π stacking.[40,86] Furthermore, photosensitizers may also be included on GFN through electrostatic interactions or covalent bonding.[66,87]

Ideally, the photosensitizers incorporated on GFN should have a high absorption in the NIR region, allowing the NIR radiation to excite both the photodynamic agent and the GFN (photothermal agent).[66] However, most of the photosensitizers incorporated so far on GFN do not have a high NIR absorption.[40,87–89] In this way, the combination photodynamic-PTT mediated by GFN commonly employs radiation with a wavelength suitable for the photosensitizer (*e.g.* 660 nm radiation for Ce6) and 808 nm radiation for the GFN[40] (Tables 1 and 2).

The photoinduced heat generated by GFN can induce the release of the loaded photosensitizers from GFN structure.[88] This phenomenon has a great importance since GFN can quench the reactive oxygen species (*e.g.* singlet oxygen) generated by the photosensitizers upon irradiation.[86–88] In this way, the NIR light induced release of the photodynamic agents, from the structure of GFN, can potentially restore their activity.
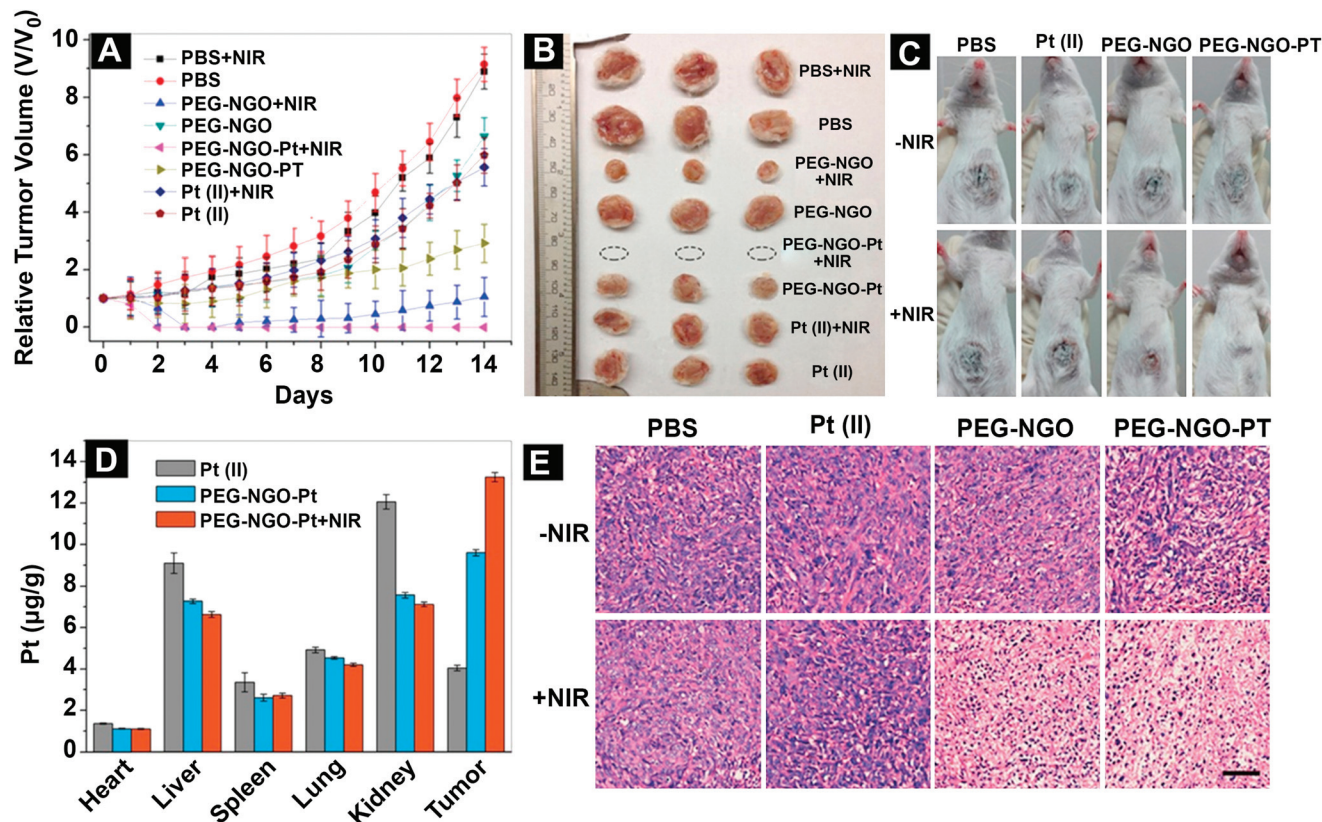
Fig. 4 *In vivo* outcome of the chemo-PTT mediated by platinum–PEG-GO complex. (A) Relative tumor volume changes of mice exposed to different treatments. Photos of the tumors (B) and mice (C) at the end point of the study. (D) Pt content in mice's major organs and tumor. (E) Hematoxylin and eosin staining of the mice's tumor tissue. Cisplatin (Pt(II)), NIR light irradiation (785 nm, 1.5 W cm^{-2}, 3 min; +NIR), Non-irradiated (-NIR), PEG-GO (PEG-NGO), Phosphate Buffered Saline (PBS), Platinum-PEG-GO complex (PEG-NGO-Pt). Reprinted from ref. 77, Copyright (2015), with permission from Elsevier.

Moreover, the temperature increase induced by GFN upon NIR laser irradiation can improve the uptake of these nanomaterials by cells.[40] In this regard, Tian *et al.* observed that the intracellular delivery of Ce6 by PEGylated GO is improved by 2–3 fold upon NIR laser irradiation.[40]

In this way, the combination photodynamic-PTT mediated by GFN can result in an enhanced therapeutic outcome (Tables 1 and 2). Dos Santos *et al.* verified that the irradiation of Pluronic F127 functionalized GO incorporating methylene blue with 660 and 808 nm lights generates a combined photodynamic–photothermal effect capable of ablating mice tumors and of preventing metastasis in major organs.[89] In contrast, the sole application of the photodynamic (methylene blue loaded GO based material + 660 nm radiation) and photothermal (methylene blue loaded GO based material + 808 nm radiation) treatments only induced a slight reduction in the tumor's growth and did not inhibit the occurrence of metastases.[89] In another work, the combined photodynamic-PTT mediated by rGO incorporating a PEGylated Ru(II) complex (photosensitizer) also induced a superior therapeutic outcome when compared to the sole application of PTT (PEG-Ru(II)/rGO plus 808 nm radiation) or photodynamic therapy (PEG-Ru(II)/rGO plus 450 nm radiation).[88]

6. PTT mediated by GFN in combination with gene therapy

GFN can be modified with polycations to enable their application in gene delivery. In this regard, GFN functionalized with poly(ethylenimine) (PEI), poly(allylamine hydrochloride) (PAH) and chitosan can form complexes with pDNA or siRNA through electrostatic interactions established between the polycations and the negatively charged groups of the genetic material.[72,90,91]

The photoinduced heat generated by GFN can further enhance their gene delivery capabilities.[72,80] In fact, the transfection efficiency mediated by GFN can be augmented by increasing cells' exposure to the NIR light.[80] For instance, Feng *et al.* verified that the PEI-PEG-GO mediated transfection of cancer cells with EGFP can be increased by up to ≈10 times upon NIR laser irradiation.[72] In other work, the photothermal transfection efficiency of PEG-PEI-rGO was also 2–3 times greater than that attained without the use of NIR light.[80] Furthermore, the conjugation of NIR light and GFN incorporating siRNA can also result in an improved gene silencing (Fig. 5).[72]

The photothermally enhanced gene transfection/silencing mediated by GFN can be explained by the improved uptake of

these nanomaterials by cells achieved after NIR laser irradiation.[72] Moreover, the photoinduced heat generated by both GO and rGO based materials can also induce the escape of these materials from the endosomes, further contributing to their improved gene transfection capabilities.[80,92] Importantly, both of these two phenomena appear to be mediated by the site-specific temperature increase mediated by GFN upon exposure to NIR light, since the direct heating of the cells at 43 °C did not result in an enhanced cellular uptake/improved endosomal escape.[72,80]

In this way, the combination of the gene delivery and PTT mediated by GFN can result in an improved therapeutic outcome (Table 1). Yin *et al.* studied the therapeutic capacity of PAH/Folic acid-PEG-GO complexed with siRNA targeting the HDAC1 and K-Ras genes.[90] When compared to mice treated with saline (control), the combined effect of the GO based material and NIR light (PTT) was able to reduce mice tumor's weight by ≈38%.[90] On the other hand, the siRNA-GO based complex (gene delivery) induced a tumor weight reduction of ≈78%.[90] In stark contrast, the combination of the siRNA-GO based complex with NIR light reduced mice tumor's weight by ≈95%,[90] thereby confirming the superior efficacy of the GFN photothermally enhanced gene delivery.

7. PTT mediated by GFN in combination with radiotherapy

The combination of GFN mediated PTT with radiotherapy is an emergent but promising approach. For this type of application, radionuclides can be labeled onto GFN, enabling internal radiotherapy.[62] In this regard, Chen *et al.* labelled PEGylated rGO with ^{131}I using the chloramine-T oxidation method.[62] On the other hand, radiosensitizers such as 5-iodo-2′-deoxyuridine (IUdR) or bismuth heteropolytungstate (BiP_5W_{30}) can also be incorporated on GFN.[76,93] These high-Z structures have an X-ray dose enhancement effect on cells, leading to an improved external radiotherapy.[94]

The temperature variation induced by GFN upon NIR irradiation can trigger the release of the loaded radiosensitizers.[93] For instance, such phenomenon takes an important role for IUdR since this thymidine analog is incorporated on DNA.[93] Moreover, GFN photoinduced heat can improve tumors' oxygenation,[76] sensitizing cancer cells to radiation-induced damage.

In this way, the application of GFN mediated radio-PTT can lead to improved therapeutic outcomes (Tables 1 and 2). Zhou and co-workers verified that poly(vinyl pyrrolidone)/BiP_5W_{30}-rGO hybrids in combination with NIR light plus X-rays could induce a tumor growth inhibition ratio of ≈98%.[76] In contrast, the effect of the hybrids plus NIR light or the hybrids plus X-rays only prompted tumor growth inhibition ratios of about 66 and 81%, respectively.[76] The sole application of the X-rays only led to a ≈39% inhibition ratio.[76] In another work, Chen *et al.* reported that the radio-PTT mediated by ^{131}I labeled PEGylated rGO could induce tumor's ablation in 4 out of 5 mice (Fig. 6).[62] On the other hand, GFN mediated internal radiotherapy (^{131}I-PEG-rGO) and GFN mediated PTT (PEG-rGO + NIR) only induced a reduction of the tumors' growth.[62]
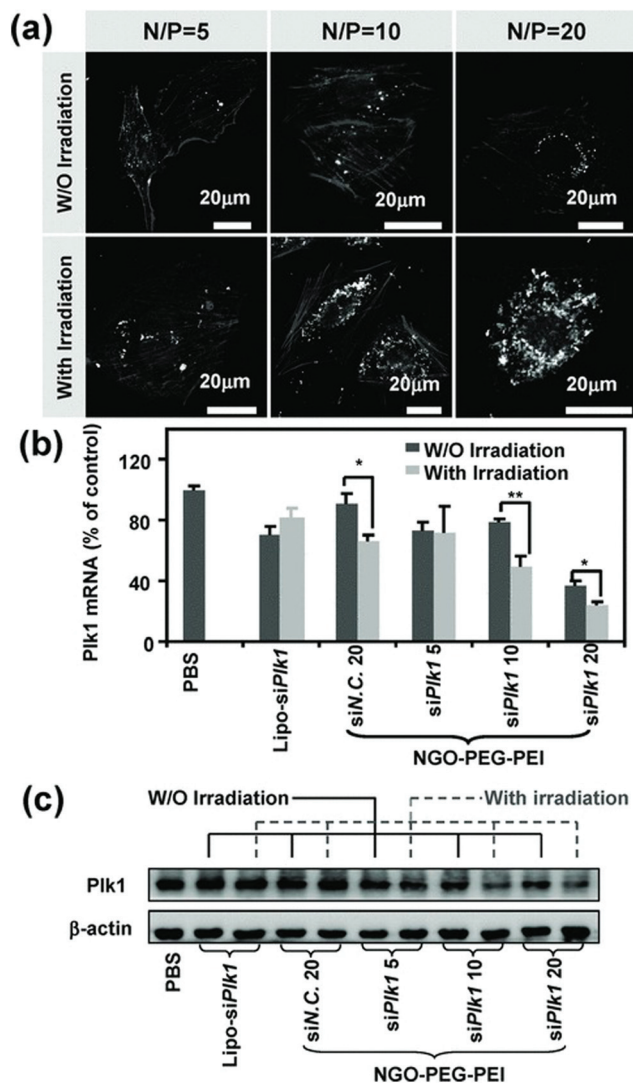

Fig. 5 Improved uptake and gene silencing mediated by PEI-PEG-GO under NIR laser irradiation. (a) Photothermally enhanced uptake of PEI-PEG-GO complexed with 6-carboxyfluorescein labelled siRNA by MDA-MB-435s cells. Plk1 mRNA (b) and protein (c) levels after treatment with PEI-PEG-GO complexed with Plk1 siRNA plus NIR light. Lipofectamine 2000 incorporating siPlk1 (Lipo-siPlk1), NIR light irradiation (808 nm, 0.5 W cm⁻², 20 min; with irradiation), PEI-PEG-GO (NGO-PEG-PEI), siRNA targeting Plk1 (siPlk1), siRNA containing a scramble sequence (siN.C.). Copyright © 2013 by John Wiley & Sons, Inc. Reprinted from ref. 72 by permission of John Wiley & Sons, Inc.

8. PTT mediated by GFN in combination with immunotherapy

Combining GFN mediated PTT with immunotherapy holds a great potential for cancer treatment. This pioneering approach
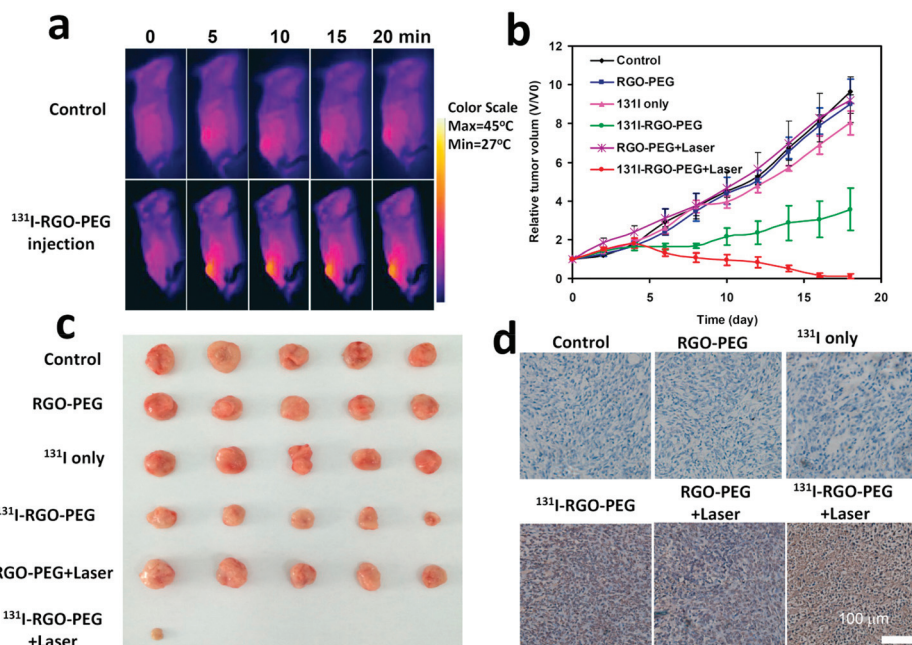
Fig. 6 *In vivo* outcome of the radio-PTT mediated by ^{131}I labeled PEGylated rGO. (a) Infrared thermal images of mice treated with ^{131}I labeled PEGylated rGO in conjugation with NIR light irradiation. (b) Relative tumor volume changes of mice exposed to different treatments and (c) respective photos of the tumors at the end point of the study. (d) Tunnel staining of the mice's tumor tissue. ^{131}I labeled PEGylated rGO (^{131}I-RGO-PEG), NIR light irradiation (808 nm, 0.2 W cm^{-2}, 20 min; +laser), PBS (Control), PEGylated rGO (RGO-PEG). Reprinted from ref. 62, Copyright (2015), with permission from Elsevier.
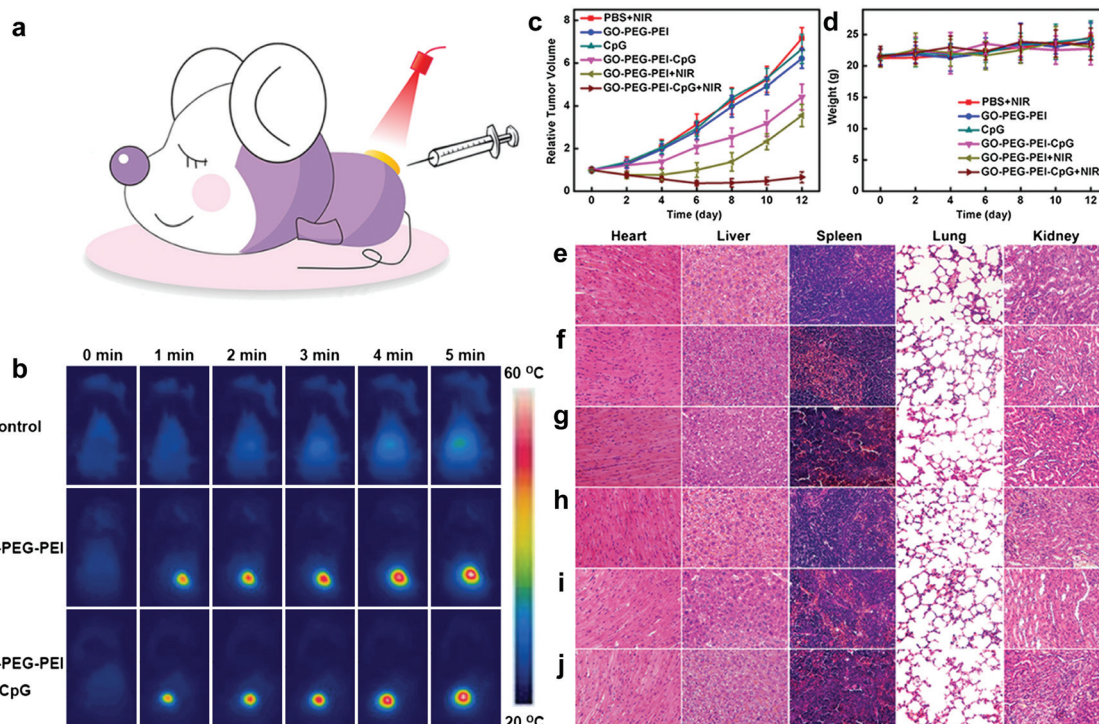

Fig. 7 *In vivo* outcome of the immuno-PTT mediated by CpG ODNs/PEI-PEG-GO nanocomplex. (a) Schematic representation of the combination immuno-PTT. (b) Infrared thermal images of mice treated CpG ODNs/PEI-PEG-GO nanocomplex plus NIR light irradiation. (c) Relative tumor volume and body weight (d) changes of mice exposed to different treatments. Hematoxylin and eosin staining of the mice's major organs after treatment with (e) PBS plus NIR radiation, (f) PEI-PEG-GO, (g) CpG ODNs, (h) CpG ODNs/PEI-PEG-GO, (i) PEI-PEG-GO plus NIR radiation and (j) CpG ODNs/ PEI-PEG-GO plus NIR radiation. CpG ODNs (CpG), CpG ODNs/PEI-PEG-GO nanocomplex (GO-PEG-PEI-CpG), NIR radiation (808 nm, 2 W cm^{-2}, 5 min; +NIR), PEI-PEG-GO (GO-PEG-PEI). Reprinted from ref. 79, Copyright (2014), with permission from Elsevier.
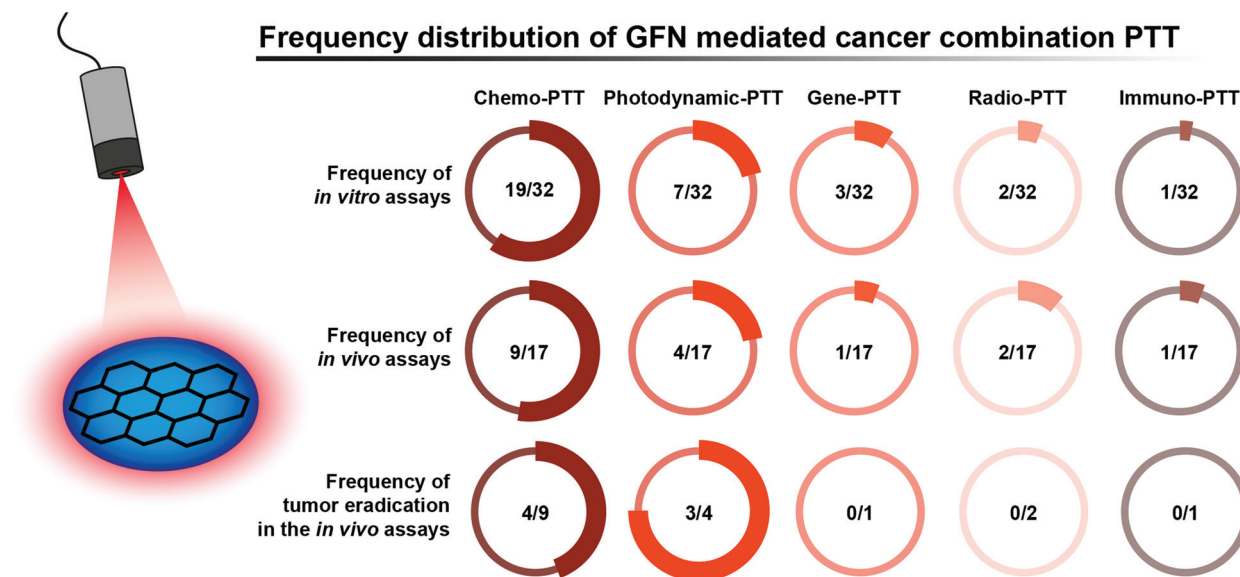
Fig. 8 Frequency distribution of GFN mediated cancer combination PTT.

was reported by Tao and co-workers which incorporated un-methylated cytosine-phosphate-guanine oligodeoxynucleotides (immunostimulatory molecules; CpG ODNs) on PEI-PEG-GO through electrostatic interactions.[79]

The authors verified that the uptake of the CpG ODNs/PEI-PEG-GO complex by macrophages cells could be increased upon NIR laser irradiation.[79] Moreover, the combination of the CpG ODNs/GFN nanocomplex with NIR light augmented macrophages' TNF-α and IL-6 secretions by about 2.2- and 1.8-fold, respectively.[79] Such enhanced immunogenicity is likely to result from the photothermally enhanced cellular uptake of the nanocomplex.[79] *In vivo*, mice treated with the GFN mediated PTT (PEI-PEG-GO + NIR light) or with the GFN mediated immunotherapy (CpG ODNs/PEI-PEG-GO nano-complex) just presented a ≈50 or 38% inhibition of the tumor's growth, respectively (Fig. 7).[79] In turn, the tumors of mice treated with the CpG ODNs/PEI-PEG-GO nanocomplex plus NIR radiation displayed a 91% growth inhibition, corro-borating the improved therapeutic outcome arising from GFN mediated immuno-PTT.[79]

9. Conclusion and outlook

The combination of GFN mediated PTT with other therapeutic modalities has been showing promising results in cancer treat-ment. Among the different GFN, GO and rGO based materials have been the most explored for this therapeutic approach. The wide application of GO and rGO in combination PTT could be explained by their simpler synthesis when compared to the other GFN. On the other hand, the enhanced photother-mal potential displayed by rGONR and rGONM should moti-vate their investigation in combination PTT.

Furthermore, the analysis of the mechanisms involved in GFN mediated combination PTT revealed that the improved

outcome arising from this therapeutic modality seems to be mainly related to the (i) photothermally enhanced cellular uptake, (ii) photothermally triggered compound release/endo-somal-escape, and (iii) combined effect of the hyperthermia *per se* with the other therapies.

Among the different combination approaches, the conju-gation of GFN mediated PTT with chemo- and photodynamic-therapies was by far the most explored by researchers (Fig. 8). Such could be related to the fact that as-synthesized GFN can directly incorporate chemotherapeutics/photosensitizers on their structure through hydrophobic–hydrophobic interactions and/or π–π stacking. Moreover, some reports also revealed that GFN mediated chemo-PTT and photodynamic-PTT were able to induce the complete eradication of mice's tumor, disclosing their high therapeutic efficacy (Fig. 8).

Regarding the combination of GFN mediated PTT with gene-, radio- and immuno-therapies, the few studies on these modal-ities revealed promising results. Nevertheless, the therapeutic capacity of these emergent combination strategies is yet insuffi-ciently explored, and thus should be further investigated.

Overall, GFN mediated PTT holds a great potential for improv-ing the efficacy of different types of therapies, which should motivate their continuous application for cancer treatment and investigation in the context of other diseases.

Conflicts of interest

The authors have no conflict of interest to declare.

Acknowledgements

References

1 N. R. Datta, S. G. Ordóñez, U. S. Gaipl, M. M. Paulides, H. Crezee, J. Gellermann, D. Marder, E. Puric and S. Bodis, *Cancer Treat. Rev.*, 2015, **41**, 742–753.

2 S. Jha, P. K. Sharma and R. Malviya, *Achiev. Life Sci.*, 2016, **10**, 161–167.

3 P. Wust, B. Hildebrandt, G. Sreenivasa, B. Rau, J. Gellermann, H. Riess, R. Felix and P. M. Schlag, *Lancet Oncol.*, 2002, **3**, 487–497.

4 W. Rao, Z. S. Deng and J. Liu, *Crit. Rev. Bioeng.*, 2010, **38**, 101–116.

5 L. Cheng, C. Wang, L. Feng, K. Yang and Z. Liu, *Chem. Rev.*, 2014, **114**, 10869–10939.

6 L. Zou, H. Wang, B. He, L. Zeng, T. Tan, H. Cao, X. He, Z. Zhang, S. Guo and Y. Li, *Theranostics*, 2016, **6**, 762–772.

7 Y. Liu, P. Bhattarai, Z. Dai and X. Chen, *Chem. Soc. Rev.*, 2019, **48**, 2053–2108.

8 C. G. Alves, D. de Melo-Diogo, R. Lima-Sousa, E. C. Costa and I. J. Correia, *Eur. J. Pharm. Biopharm.*, 2019, **137**, 86–94.

9 A. F. Moreira, D. R. Dias, E. C. Costa and I. J. Correia, *Eur. J. Pharm. Sci.*, 2017, **104**, 42–51.

10 R. K. Jain and T. Stylianopoulos, *Nat. Rev. Clin. Oncol.*, 2010, **7**, 653–664.

11 M. J. Ernsting, M. Murakami, A. Roy and S.-D. Li, *J. Controlled Release*, 2013, **172**, 782–794.

12 D. de Melo-Diogo, C. Pais-Silva, D. R. Dias, A. F. Moreira and I. J. Correia, *Adv. Healthcare Mater.*, 2017, **6**, 1700073.

13 Y. Wei, L. Quan, C. Zhou and Q. Zhan, *Nanomedicine*, 2018, **13**, 1495–1512.

14 W. Sheng, S. He, W. J. Seare and A. Almutairi, *J. Biomed. Opt.*, 2017, **22**, 080901.

15 C. G. Alves, R. Lima-Sousa, D. de Melo-Diogo, R. O. Louro and I. J. Correia, *Int. J. Pharm.*, 2018, **542**, 164–175.

16 A. Vogel and V. Venugopalan, *Chem. Rev.*, 2003, **103**, 577–644.

17 C. Pais-Silva, D. de Melo-Diogo and I. J. Correia, *Eur. J. Pharm. Biopharm.*, 2017, **113**, 108–117.

18 W. Yin, L. Yan, J. Yu, G. Tian, L. Zhou, X. Zheng, X. Zhang, Y. Yong, J. Li, Z. Gu and Y. Zhao, *ACS Nano*, 2014, **8**, 6922–6933.

19 G. Tian, X. Zhang, X. Zheng, W. Yin, L. Ruan, X. Liu, L. Zhou, L. Yan, S. Li, Z. Gu and Y. Zhao, *Small*, 2014, **10**, 4160–4170.

20 X.-R. Song, X. Wang, S.-X. Yu, J. Cao, S.-H. Li, J. Li, G. Liu, H.-H. Yang and X. Chen, *Adv. Mater.*, 2015, **27**, 3285–3291.

21 J. Kim, J. Kim, C. Jeong and W. J. Kim, *Adv. Drug Delivery Rev.*, 2016, **98**, 99–112.

22 T. Bao, W. Yin, X. Zheng, X. Zhang, J. Yu, X. Dong, Y. Yong, F. Gao, L. Yan, Z. Gu and Y. Zhao, *Biomaterials*, 2016, **76**, 11–24.

23 D. de Melo-Diogo, C. Pais-Silva, E. C. Costa, R. O. Louro and I. J. Correia, *Nanomedicine*, 2017, **12**, 443–456.

24 A. Saneja, R. Kumar, D. Arora, S. Kumar, A. K. Panda and S. Jaglan, *Drug Discovery Today*, 2018, **23**, 1115–1125.

25 A. F. Moreira, C. F. Rodrigues, C. A. Reis, E. C. Costa, P. Ferreira and I. J. Correia, *Nanomedicine*, 2018, **13**, 2611–2627.

26 J.-L. Li, B. Tang, B. Yuan, L. Sun and X.-G. Wang, *Biomaterials*, 2013, **34**, 9519–9534.

27 Y. Yang, A. M. Asiri, Z. Tang, D. Du and Y. Lin, *Mater. Today*, 2013, **16**, 365–373.

28 G. Gonçalves, M. Vila, M.-T. Portolés, M. Vallet-Regi, J. Gracio and P. A. A. P. Marques, *Adv. Healthcare Mater.*, 2013, **2**, 1072–1090.

29 J. Liu, L. Cui and D. Losic, *Acta Biomater.*, 2013, **9**, 9243–9257.

30 S. Goenka, V. Sant and S. Sant, *J. Controlled Release*, 2014, **173**, 75–88.

31 Y. Li, H. Dong, Y. Li and D. Shi, *Int. J. Nanomed.*, 2015, **10**, 2451–2459.

32 D. de Melo-Diogo, R. Lima-Sousa, C. G. Alves, E. C. Costa, R. O. Louro and I. J. Correia, *Colloids Surf., B*, 2018, **171**, 260–275.

33 K. Yang, S. Zhang, G. Zhang, X. Sun, S.-T. Lee and Z. Liu, *Nano Lett.*, 2010, **10**, 3318–3323.

34 K. Yang, J. Wan, S. Zhang, B. Tian, Y. Zhang and Z. Liu, *Biomaterials*, 2012, **33**, 2206–2214.

35 K. Yang, L. Hu, X. Ma, S. Ye, L. Cheng, X. Shi, C. Li, Y. Li and Z. Liu, *Adv. Mater.*, 2012, **24**, 1868–1872.

36 C. Jang, J. H. Lee, A. Sahu and G. Tae, *Nanoscale*, 2015, **7**, 18584–18594.

37 J. H. Lee, A. Sahu, C. Jang and G. Tae, *J. Controlled Release*, 2015, **209**, 219–228.

38 X. Sun, Z. Liu, K. Welsher, J. T. Robinson, A. Goodwin, S. Zaric and H. Dai, *Nano Res.*, 2008, **1**, 203–212.

39 L. Zhang, J. Xia, Q. Zhao, L. Liu and Z. Zhang, *Small*, 2010, **6**, 537–544.

40 B. Tian, C. Wang, S. Zhang, L. Feng and Z. Liu, *ACS Nano*, 2011, **5**, 7000–7009.

41 A. Deb and R. Vimala, *J. Drug Delivery Sci. Technol.*, 2018, **43**, 333–342.

42 Y. Zhu, S. Murali, W. Cai, X. Li, J. W. Suk, J. R. Potts and R. S. Ruoff, *Adv. Mater.*, 2010, **22**, 3906–3924.

43 D. Chen, H. Feng and J. Li, *Chem. Rev.*, 2012, **112**, 6027–6053.

44 R. K. Singh, R. Kumar and D. P. Singh, *RSC Adv.*, 2016, **6**, 64993–65011.

45 W. S. Hummers Jr. and R. E. Offeman, *J. Am. Chem. Soc.*, 1958, **80**, 1339–1339.

46 D. C. Marcano, D. V. Kosynkin, J. M. Berlin, A. Sinitskii, Z. Sun, A. Slesarev, L. B. Alemany, W. Lu and J. M. Tour, *ACS Nano*, 2010, **4**, 4806–4814.

47 Z. Liu, J. T. Robinson, X. Sun and H. Dai, *J. Am. Chem. Soc.*, 2008, **130**, 10876–10877.

48 H. Shen, M. Liu, H. He, L. Zhang, J. Huang, Y. Chong, J. Dai and Z. Zhang, *ACS Appl. Mater. Interfaces*, 2012, **4**, 6317–6323.

49 D. de Melo-Diogo, E. C. Costa, C. G. Alves, R. Lima-Sousa, P. Ferreira, R. O. Louro and I. J. Correia, *Eur. J. Pharm. Biopharm.*, 2018, **131**, 162–169.

50 J. T. Robinson, S. M. Tabakman, Y. Liang, H. Wang, H. Sanchez Casalongue, D. Vinh and H. Dai, *J. Am. Chem. Soc.*, 2011, **133**, 6825–6831.

51 R. Lima-Sousa, D. de Melo-Diogo, C. G. Alves, E. C. Costa, P. Ferreira, R. O. Louro and I. J. Correia, *Carbohydr. Polym.*, 2018, **200**, 93–99.

52 O. Akhavan, E. Ghaderi, S. Aghayee, Y. Fereydooni and A. Talebi, *J. Mater. Chem.*, 2012, **22**, 13773–13781.

53 H. Kim, D. Lee, J. Kim, T.-i. Kim and W. J. Kim, *ACS Nano*, 2013, **7**, 6735–6746.

54 J. Chen, H. Liu, C. Zhao, G. Qin, G. Xi, T. Li, X. Wang and T. Chen, *Biomaterials*, 2014, **35**, 4986–4995.

55 O. Akhavan, E. Ghaderi and H. Emamy, *J. Mater. Chem.*, 2012, **22**, 20626–20633.

56 D. V. Kosynkin, A. L. Higginbotham, A. Sinitskii, J. R. Lomeda, A. Dimiev, B. K. Price and J. M. Tour, *Nature*, 2009, **458**, 872–876.

57 O. Akhavan and E. Ghaderi, *Small*, 2013, **9**, 3593–3601.

58 X. Zhang, J. Yin, C. Peng, W. Hu, Z. Zhu, W. Li, C. Fan and Q. Huang, *Carbon*, 2011, **49**, 986–995.

59 K. Yang, J. Wan, S. Zhang, Y. Zhang, S.-T. Lee and Z. Liu, *ACS Nano*, 2011, **5**, 516–522.

60 K. Yang, H. Gong, X. Shi, J. Wan, Y. Zhang and Z. Liu, *Biomaterials*, 2013, **34**, 2787–2795.

61 S. Zhang, K. Yang, L. Feng and Z. Liu, *Carbon*, 2011, **49**, 4040–4049.

62 L. Chen, X. Zhong, X. Yi, M. Huang, P. Ning, T. Liu, C. Ge, Z. Chai, Z. Liu and K. Yang, *Biomaterials*, 2015, **66**, 21–28.

63 Z. Sheng, L. Song, J. Zheng, D. Hu, M. He, M. Zheng, G. Gao, P. Gong, P. Zhang, Y. Ma and L. Cai, *Biomaterials*, 2013, **34**, 5236–5243.

64 H.-W. Yang, Y.-J. Lu, K.-J. Lin, S.-C. Hsu, C.-Y. Huang, S.-H. She, H.-L. Liu, C.-W. Lin, M.-C. Xiao, S.-P. Wey, P.-Y. Chen, T.-C. Yen, K.-C. Wei and C.-C. M. Ma, *Biomaterials*, 2013, **34**, 7204–7214.

65 L. Hou, Q. Feng, Y. Wang, H. Zhang, G. Jiang, X. Yang, J. Ren, X. Zhu, Y. Shi and Z. Zhang, *J. Nanopart. Res.*, 2015, **17**, 162.

66 S. Luo, Z. Yang, X. Tan, Y. Wang, Y. Zeng, Y. Wang, C. Li, R. Li and C. Shi, *ACS Appl. Mater. Interfaces*, 2016, **8**, 17176–17186.

67 J. Fang, H. Nakamura and H. Maeda, *Adv. Drug Delivery Rev.*, 2011, **63**, 136–151.

68 Y. Matsumoto, J. W. Nichols, K. Toh, T. Nomoto, H. Cabral, Y. Miura, R. J. Christie, N. Yamada, T. Ogura, M. R. Kano, Y. Matsumura, N. Nishiyama, T. Yamasoba, Y. H. Bae and K. Kataoka, *Nat. Nanotechnol.*, 2016, **11**, 533–538.

69 C. Chung, Y.-K. Kim, D. Shin, S.-R. Ryoo, B. H. Hong and D.-H. Min, *Acc. Chem. Res.*, 2013, **46**, 2211–2224.

70 Y.-W. Chen, Y.-L. Su, S.-H. Hu and S.-Y. Chen, *Adv. Drug Delivery Rev.*, 2016, **105**, 190–204.

71 D. Bitounis, H. Ali-Boucetta, B. H. Hong, D.-H. Min and K. Kostarelos, *Adv. Mater.*, 2013, **25**, 2258–2268.

72 L. Feng, X. Yang, X. Shi, X. Tan, R. Peng, J. Wang and Z. Liu, *Small*, 2013, **9**, 1989–1997.

73 W. Miao, G. Shim, C. M. Kang, S. Lee, Y. S. Choe, H.-G. Choi and Y.-K. Oh, *Biomaterials*, 2013, **34**, 9638–9647.

74 K. F. Chu and D. E. Dupuy, *Nat. Rev. Cancer*, 2014, **14**, 199–208.

75 S. Gao, M. Zheng, X. Ren, Y. Tang and X. Liang, *Oncotarget*, 2016, **7**, 57367–57378.

76 R. Zhou, H. Wang, Y. Yang, C. Zhang, X. Dong, J. Du, L. Yan, G. Zhang, Z. Gu and Y. Zhao, *Biomaterials*, 2019, **189**, 11–22.

77 J. Li, Z. Lyv, Y. Li, H. Liu, J. Wang, W. Zhan, H. Chen, H. Chen and X. Li, *Biomaterials*, 2015, **51**, 12–21.

78 N. Frazier and H. Ghandehari, *Biotechnol. Bioeng.*, 2015, **112**, 1967–1983.

79 Y. Tao, E. Ju, J. Ren and X. Qu, *Biomaterials*, 2014, **35**, 9963–9971.

80 H. Kim and W. J. Kim, *Small*, 2014, **10**, 117–126.

81 R. K. Thapa, Y. Choi, J.-H. Jeong, Y. S. Youn, H.-G. Choi, C. S. Yong and J. O. Kim, *Pharm. Res.*, 2016, **33**, 2815–2827.

82 L. Feng, K. Li, X. Shi, M. Gao, J. Liu and Z. Liu, *Adv. Healthcare Mater.*, 2014, **3**, 1261–1271.

83 S.-H. Hu, R.-H. Fang, Y.-W. Chen, B.-J. Liao, I.-W. Chen and S.-Y. Chen, *Adv. Funct. Mater.*, 2014, **24**, 4144–4155.

84 T. Yin, J. Liu, Z. Zhao, Y. Zhao, L. Dong, M. Yang, J. Zhou and M. Huo, *Adv. Funct. Mater.*, 2017, **27**, 1604620.

85 J. Shi, L. Wang, J. Zhang, R. Ma, J. Gao, Y. Liu, C. Zhang and Z. Zhang, *Biomaterials*, 2014, **35**, 5847–5861.

86 Y. Wang, H. Wang, D. Liu, S. Song, X. Wang and H. Zhang, *Biomaterials*, 2013, **34**, 7715–7724.

87 A. Sahu, W. I. Choi, J. H. Lee and G. Tae, *Biomaterials*, 2013, **34**, 6239–6248.

88 D.-Y. Zhang, Y. Zheng, C.-P. Tan, J.-H. Sun, W. Zhang, L.-N. Ji and Z.-W. Mao, *ACS Appl. Mater. Interfaces*, 2017, **9**, 6761–6771.

89 M. S. C. dos Santos, A. L. Gouvêa, L. D. de Moura, L. G. Paterno, P. E. N. de Souza, A. P. Bastos, E. A. M. Damasceno, F. H. Veiga-Souza, R. B. de Azevedo and S. N. Báo, *J. Nanobiotechnol.*, 2018, **16**, 9.

90 F. Yin, K. Hu, Y. Chen, M. Yu, D. Wang, Q. Wang, K.-T. Yong, F. Lu, Y. Liang and Z. Li, *Theranostics*, 2017, **7**, 1133–1148.

91 H. Bao, Y. Pan, Y. Ping, N. G. Sahoo, T. Wu, L. Li, J. Li and L. H. Gan, *Small*, 2011, **7**, 1569–1578.

92 H. Kim, J. Kim, M. Lee, H. C. Choi and W. J. Kim, *Adv. Healthcare Mater.*, 2016, **5**, 1918–1930.

93 S. Kargar, S. Khoei, S. Khoee, S. Shirvalilou and S. R. Mahdavi, *Photodiagn. Photodyn. Ther.*, 2018, **21**, 91–97.

94 P. Retif, S. Pinel, M. Toussaint, C. Frochot, R. Chouikrat, T. Bastogne and M. Barberi-Heyob, *Theranostics*, 2015, **5**, 1030–1044.

95 W. Zhang, Z. Guo, D. Huang, Z. Liu, X. Guo and H. Zhong, *Biomaterials*, 2011, **32**, 8555–8561.

96 Y.-J. Lu, C.-W. Lin, H.-W. Yang, K.-J. Lin, S.-P. Wey, C.-L. Sun, K.-C. Wei, T.-C. Yen, C.-I. Lin, C.-C. M. Ma and J.-P. Chen, *Carbon*, 2014, **74**, 83–95.

97 R. K. Thapa, J. Y. Choi, B. K. Poudel, H.-G. Choi, C. S. Yong and J. O. Kim, *Int. J. Nanomed.*, 2016, **11**, 2799–2813.

98 X. C. Qin, Z. Y. Guo, Z. M. Liu, W. Zhang, M. M. Wan and B. W. Yang, *J. Photochem. Photobiol., B*, 2013, **120**, 156–162.

99 T. H. Tran, H. T. Nguyen, T. T. Pham, J. Y. Choi, H.-G. Choi, C. S. Yong and J. O. Kim, *ACS Appl. Mater. Interfaces*, 2015, **7**, 28647–28655.

100 Q. Li, L. Hong, H. Li and C. Liu, *Biosens. Bioelectron.*, 2017, **89**, 477–482.